CONFERENCE PRE-PRINT

OVERVIEW OF THE MAST UPGRADE PHYSICS PROGRAMME: TESTING NOVEL CONCEPTS AT LOW ASPECT RATIO TO INFORM FUTURE DEVICES

J. R. Harrison¹, A. Aboutaleb², M. Aljunid¹, R. Allan¹, S. Y. Allan¹, E. Alli¹, H. Anand³, Y. Andrew⁴, L. C. Appel¹, A. Ash¹, J. Ashton¹, F. Auriemma⁵, O. Bachmann¹, P. Balazs⁶, O. Bardsley¹, M. Barnes⁷, B. Barrett¹, D. Baver⁸, C. Beckley¹, J. Bennett¹, J. Bentley¹, J. Berkery⁹, M. Bernert¹⁰, N. Bertelli⁹, S. Blackmore¹, A. Bock¹⁰, W. Boeglin², J. Booth¹, A. Bosnjak¹, C. Bowman¹, J. Bradley¹¹, D. Brida¹⁰, M. Brix¹, P. K. Browning¹², J. Bryant¹¹, P. Bryant¹¹, J. Buchanan¹, M. Bull¹, N. Bulmer¹, D. Burke¹, P. Cahill¹, A. Carruthers¹, L. Casali¹³, A. Cassidy¹, M. Cecconello^{14,15}, B. Chamberlain¹, B. Chapman¹, R. Chazal¹, Z. P. Chen¹⁶, M. Clark¹, T. Clayton¹, K. Collie¹, D. Collishaw-Schepman¹, J. W. Connor¹, M. Coy¹, S. Cramp¹, N. Crocker¹⁷, D. Cruse¹, G. Cunningham¹, I. Cziegler¹⁸, Y. Damizia^{11,19}, K. Davies¹, P. Davies¹, I. Day¹, E. Delabie²⁰, G. L. Derks^{21,22}, S. Dixon¹, J. Dobrashian¹, M. Dreval²³, X. Du³, H. Dudding¹, D. Dunai⁶, M. Dunne¹⁰, J. Edmond¹, J. Edwards¹, S. Elmore¹, Y. Enters¹⁸, M. Faitsch¹⁰, F. Federici²⁰, N. Fedorczak²⁴, F. Felici²⁵, A. R. Field¹, I. FitzGerald¹, M. Fitzgerald¹, R. Fitzpatrick¹⁶, S. Frankel¹, L. Frassinetti²⁶, S. Freethy¹, W. Fuller²⁷, S. Gabriellini¹, K. Gage¹⁷, J. Galdon-Quiroga²⁸, C. Garner¹, L. Garzotti¹, K. J. Gibson¹⁸, C. Gibson¹, C. Giroud¹, J. Goatley¹, A. Goodyear¹, M. Gorelenkova⁹, S. Gosden¹, J. P. Graves^{18,25}, D. Greenhouse^{18,29}, R. Griffiths¹, C. J. Ham¹, E. Harrington¹, R. Harrison¹, A. Haupt¹, J. Hawes¹, S. Hegedus⁶, S. S. Henderson¹, C. Hickling¹, M. Hill¹, B. Hnat³⁰, C. Hogben¹, B. Honey¹, L. Howlett¹, Z. Huang¹, J. Hughes³¹, R. Hussain¹, K. Imada^{3,18}, P. Ivanov¹, A. Jackson², P. Jacquet¹, P. Jepson¹, P. Jones¹, T. Jones¹, M. Juvonen¹, V. Kachkanov¹, B. Kandan¹, I. Katramados¹, S. Kaye⁹, Y. O. Kazakov³², D. Keeling¹, D. Kennedy¹, A. Kenny¹, H-T. Kim¹, R. King¹, A. King¹, D. King¹, V. Kiptily¹, A. Kirk¹, A. Kleiner⁹, M. Knolker³, M. Kochan¹, L. Kogan¹, B. Kool^{21,22}, D. Kos¹, M. Kotschenreuther¹⁶, M. Lampert⁹, A. Lawson¹, K. Lawson¹, G. Lee¹, K. -W. Lee¹³, M. Lees¹, S. Leigh¹, A. W. Leonard³, G. Liddiard¹, B. Lipschultz¹⁸, E. Litherland-Smith¹, Y. Q. Liu³, B. A. Lomanowski²⁰, N. Lonigro^{1,18}, J. Lore²⁰, J. Lovell²⁰, R. Lucock¹, T. Luong¹⁷, J. Macdonald¹, T. Macwan³³, S. Mahajan¹⁶, F. Maiden¹⁸, R. Maingi⁹, C. Man-Friel¹, F. Mansfield¹, S. Marsden¹, R. Martin¹, R. Mathew¹, R. Maurizio³, U. Mazzarese¹, S. Mazzi²⁵, R. McAdams¹, G. McArdle¹, J. McBride¹, K. McClements¹, J. McClenaghan³, D. McConville¹, K. McKay¹¹, P. McKnight¹, C. McKnight¹, A. McLean³³, B. F. McMillan³⁰, A. McShee¹, J. Measures¹, N. Mehay¹, S. Menmuir¹, H. F. Meyer¹, C. A. Michael¹⁷, F. Militello¹, J. Mitchell¹, P. Monaghan¹, R. Mooney¹, N. Mooring¹, R. Morales Gomes¹, D. Morbey¹, S. Mordijck¹⁹, C. Morgan¹, D. Moulton¹, S. Munaretto⁹, A. Munasinghe¹, O. Myatra¹, A. O. Nelson³⁴, M. Nicassio¹, M. G. O'Mullane³⁵, C. Olde¹, H. J. Oliver¹, P. Ollus³⁶, J. Omotani¹, M. Ono⁹, R. Osawa¹, T. Osborne³, N. Osborne^{1,11}, R. Otin¹, E. Ozturk^{19,37}, F. Palermo¹, A. Pankin⁹, I. Paradela Pérez²⁰, J. Parisi⁹, E. Parr¹, B. Parry¹, B. S. Patel¹, D. Payne¹, C. Paz-Soldan³⁴, A. Phelps³⁵, C. Piron³⁸, L. Piron³⁹, R. Preece¹, M. Price¹, B. Pritchard¹⁸, R. Proudfoot¹, G. Pucella³⁸, T. Pumfrett¹, H. Reimerdes²⁵, T. Rhodes¹⁷, E. Ribeiro¹, J. Riquezes³⁴, J. F. Rivero-Rodriguez^{1,40}, J. Roberts¹, M. Robson¹, K. Ronald³⁵, E. Rose¹, D. Ryan¹, P. Ryan¹, S. Saarelma¹, S. Sabbagh³⁴, R. Sarwar¹, P. Saunders¹, O. Sauter²⁵, R. Scannell¹, R. Sealey¹, R. Seath¹, S. Sharapov¹, R. Sharma¹, H. Sheikh¹, S. Shiraiwa⁹, B. Sieglin¹⁰, S. A. Silburn¹, M. Simmonds¹, J. Simpson¹, A. Sladkomedova⁴¹, J. Smith¹, P. Smith¹, V. A. Soukhanovskii³³, D. Speirs³⁵, C. Srinivasan¹, G. Staebler²⁰, R. Stephen¹, P. Stevenson¹, J. Stobbs¹⁰, C. Stroud¹, H. Sun¹, G. Szepesi¹, C. Tame¹, C. Theiler²⁵, S. Thomas³¹, S. Thomas¹, B. Thomas¹, N. Thomas-Davies¹, K. Thome³, A. J. Thornton¹, A. Tilley¹, I. Tirkova¹, M. Tobin³⁴, P. Tonner¹, A. Tookey¹, G. Tvalashvili¹, V. H. Vall-Chen⁴², M. Vallar²⁵, M. Valovic¹, R. G. L. Vann¹⁸, L. Velarde²⁸, K. Verhaegh²², E. Viezzer⁴³, C. Vincent¹, C. Vincent¹, M. Walsh¹, T. Walsh¹, M. Warr¹, W. Wehner³, S. Wiesen⁴⁴, T. A. Wijkamp^{21,22}, D. Wilkins¹, J. Willis¹, H. R. Wilson¹, T. Wilson¹, N. Winston¹, G. Withenshaw¹, H. Wong¹⁷, M. Wood¹, R. Worrall¹, Q. Xia¹, L. Xiang¹, G. Xiang¹, T. Xu¹, V. Zamkovska³⁴

¹ UKAEA (United Kingdom Atomic Energy Authority), Culham Campus, Abingdon, Oxfordshire, OX14 3DB, UK.

² Department of Physics, Florida International University, 11200 SW, Miami, FL 33199, USA

³ General Atomics, PO Box 85608, San Diego, CA 92186-5608, USA

⁴ Blackett Laboratory, Imperial College London - London, SW7 2BW, UK

⁵ Consorzio RFX (CNR, ENEA, INFN, Università di Padova, Acciaierie Venete SpA), Corso Stati Uniti 4, 35127 Padova, Italy

⁶ HUN-REN Centre for Energy Research, Budapest, Hungary

⁷ Rudolf Peierls Centre for Theoretical Physics, University of Oxford, Oxford OX1 3NP, United Kingdom

⁸ Astrodel

⁹ Princeton Plasma Physics Laboratory, Princeton, NJ, USA

¹⁰ Max-Planck-Institut fur Plasmaphysik, 85748 Garching, Germany

- ¹¹ Department of Electrical Engineering and Electronics, University of Liverpool, Brownlow Hill, Liverpool, L69 3GJ, United Kingdom
- ¹² Department of Physics and Astronomy, University of Manchester, Oxford Road, Manchester M13 9PL, UK
- ¹³ University of Tennessee, Knoxville, Knoxville, TN 37996, United States of America
- ¹⁴ Department of Physics, Durham University, Durham DH1 3LE, United Kingdom
- ¹⁵ Department of Physics and Astronomy, Uppsala University, Uppsala SE-75105, Sweden
- ¹⁶ Institute for Fusion Studies, The University of Texas at Austin, Austin, TX, United States of America
- ¹⁷ Physics and Astronomy Dept., University of California, Los Angeles, California 90098 USA
- ¹⁸ York Plasma Institute, Department of Physics, University of York, Heslington, York YO10 5DD, United Kingdom
- ¹⁹ Dept. of Computer Science, College of William & Mary, Williamsburg, VA, US
- ²⁰ Oak Ridge National Laboratory, Oak Ridge, Tennessee 37831, USA
- ²¹ Dutch Institute for Fundamental Energy Research DIFFER, Eindhoven, Netherlands
- ²² Eindhoven University of Technology, Eindhoven, Netherlands
- ²³ National Science Center 'Kharkov Institute of Physics and Technology', Akademichna 1, Kharkiv 61108, Ukraine
- ²⁴ CEA, IRFM, F-13108 Saint-Paul-lez-Durance, France
- ²⁵ Ecole Polytechnique Fédérale de Lausanne (EPFL), Swiss Plasma Center (SPC), CH-1015 Lausanne, Switzerland
- ²⁶ Division of Fusion Plasma Physics, KTH Royal Institute of Technology, Stockholm SE-100 44, Sweden
- ²⁷ Department of Physics, University of Warwick, Coventry CV4 7AL, United Kingdom of Great Britain and Northern Ireland
- ²⁸ Dept. of Atomic, Molecular and Nuclear Physics, University of Seville, Avda. Reina Mercedes, 41012 Seville, Spain
- ²⁹ digiLab, The Quay, Exeter EX2 4AN, United Kingdom
- ³⁰ Department of Physics, University of Warwick, Coventry, CV4 7AL, United Kingdom
- ³¹ Plasma Science and Fusion Center, Massachusetts Institute of Technology, Cambridge, Massachusetts 02139, USA
- ³² Laboratory for Plasma Physics, LPP-ERM/KMS, TEC Partner, Brussels, Belgium
- ³³ Lawrence Livermore National Laboratory, Livermore, CA, USA
- ³⁴ Department of Applied Physics and Applied Mathematics, Columbia University, New York, NY, USA
- ³⁵ Department of Physics, SUPA, University of Strathclyde, Glasgow, Scotland, U.K.
- ³⁶ Department of Applied Physics, Aalto University, PO Box 11100, 00076 Aalto, Finland
- ³⁷ Department of Computing, Imperial College, Prince Consort Road, London SW7 2BZ, United Kingdom of Great Britain and Northern Ireland
- ³⁸ ENEA, Fusion and Nuclear Safety Department, C. R. Frascati, Via E. Fermi 45, 00044, Frascati, Roma, Italy
- ³⁹ Dipartimento di Fisica "G. Galilei", Università degli Studi di Padova, Padova, Italy

Consorzio RFX, Corso Stati Uniti 4, 35127, Padova, Italy

- ⁴⁰ Department of Mechanical Engineering and Manufacturing, Universidad de Sevilla, Seville, 81, 41004, Spain
- ⁴¹ Tokamak Energy Ltd., 173 Brook Drive, Milton Park, Oxfordshire, OX14 4SD, United Kingdom
- ⁴² Institute of High Performance Computing A*STAR, Singapore
- ⁴³ Departamento de Física Atómica, Molecular y Nuclear, Universidad de Sevilla, Sevilla, Spain
- ⁴⁴ Forschungszentrum Jülich GmbH, Institut für Energie- und Klimaforschung—Plasmaphysik, 52425 Jülich, Germany

Abstract

Recent results from the MAST Upgrade (MAST-U) spherical tokamak are presented, with an emphasis on aspects that are unique and novel, to deepen understanding of key plasma physics issues governing the operation of ITER and the design of future fusion power plants. Robust, high performance plasma scenarios have been developed to facilitate the wider science programme. Confinement in these scenarios is constrained by the presence of m/n = 2/1 modes that cause substantial losses of fast ions. The electron temperature at the pedestal top, $T_{e,ped}$ is constrained to $T_{e,ped} < 350$ eV to maintain regular ELMs. In studies of energetic particle physics, losses of fast particles due to Global Alfvén Eigenmodes have been identified. Losses of neutral beam heating due to interactions with main chamber neutrals have been estimated to be up to 50% for the off-axis beam, emphasising the need to reduce the main chamber neutral density. First measurements have been performed with a diamond proton detector, exhibiting improved resilience to the operational conditions in a tokamak. In studies of MHD stability, it has been shown that the onset of the performance-limiting 2/1 mode is coincident with the q=2 flux surface residing in a local minimum of the current density profile. Transiently avoiding the 2/1 mode can result in a $\sim 15\%$ improvement in β_N . In plasma scenarios with strong neutral beam heating, the central safety factor is constrained to ~ 1 in the absence of sawteeth, indicating the presence of a flux pumping mechanism. The operational space where flux pumping is evident has been characterised. In studies of pedestal physics, it has been found that main chamber neutrals tend to elevate the pedestal top density and reduce the pedestal top electron temperature. The operational space of spherical tokamaks to stationary small

ELM and ELM-free regimes has been expanded. Strong shaping of the last closed flux surface can induce a transition from large to small ELMs, and ELM suppression with Resonant Magnetic Perturbations has been observed for the first time in a spherical tokamak. Negative triangularity shaping has been explored to induce a transition from ELMy H-mode to a high-performance L-mode regime. Studies of plasma exhaust have demonstrated the advantages of tightly baffled divertors on scenario integration and real-time control. Integration of a high-performance plasma core with detached outer divertors has been demonstrated in the X-point target configuration. A newly commissioned lower divertor cryopump reduces the lower divertor neutral pressure by up to 50%, with minimal effect on the main chamber or upper divertor. New measurements and SOLPS-ITER simulations emphasise the importance of plasma-neutral interactions on divertor detachment in the conditions accessible in experiments. Real-time detachment control of the ionisation front location in both divertors has been demonstrated in double null experiments, showing that the tightly baffled divertors uniquely enable independent control of the detachment state of each divertor.

1. INTRODUCTION

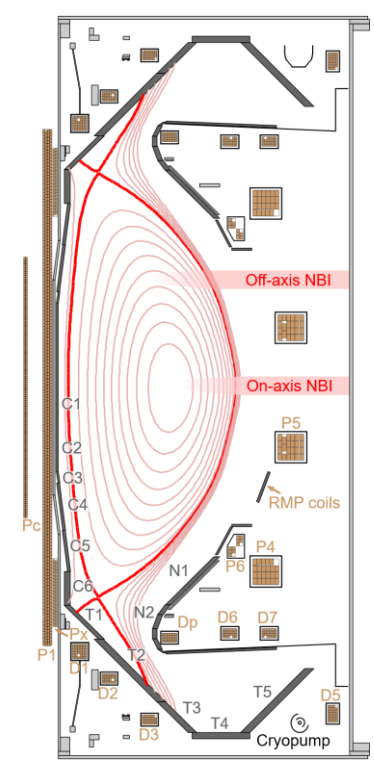


Figure 1: Poloidal cross-section of MAST Upgrade. The components in the lower half of the machine are labelled, which is identical to their counterparts in the upper half.

MAST Upgrade (shown schematically in Figure 1) is a low aspect ratio tokamak (major radius / minor radius (R/a) = 0.85/0.65 ~1.3, plasma current (I_p) ≤ 2.0 MA, toroidal field on axis (B_{ϕ}) ≤ 0.8 T, pulse length ≤ 5 s) and one of the largest spherical tokamaks worldwide, together with NSTX-U [1]. Key features include 22 poloidal field coils to provide considerable flexibility to independently vary the shape of the plasma core and divertors within tightly baffled chambers utilising 22 poloidal field coils. Coils to produce non-axisymmetic fields for ELM control with Resonant Magnetic Perturbations (RMPs) and correcting for intrinsic error fields are available, with two rows of in-vessel coils (four equally spaced toroidally above the mid-plane, eight below) and two pairs of exvessel coils respectively. On- and off-axis Neutral Beam Injectors (NBI) provide strong sources of heat and momentum to the plasma and enable studies of the confinement of super Alfvénic fast ions that more closely mimics the confinement of fusion products. An extensive suite of diagnostics is available to support a broad and deep physics programme in these key physics issues for the operation of ITER and the design of future power plants including DEMO [2] and STEP [3].

Recent physics results from MAST Upgrade make significant and unique advances in understanding key physics issues governing the operation of ITER and future fusion power plants. The operating space has expanded considerably thanks to new capabilities including an active lower divertor cryopump to control the neutral pressure and sophisticated real-time equilibrium shape control to reach higher elongation ($\kappa \sim 1.8 \rightarrow 2.5$) and a larger range of triangularity ($\delta \sim -0.15 \rightarrow 0.5$), reaching negative triangularity for the first time in a spherical tokamak. Operation with Super-X divertor configurations in the attached regime has been achieved with the cryopumped divertor, enabling studies of detachment onset. The

plasma conditions in the divertors and main chamber can be effectively decoupled, due to the tightly baffled divertor chambers, which is rarely observed in current devices and enables pioneering studies of core-edge-divertor integration. On- and off-axis Neutral Beam Injectors (NBI) enable studies of the confinement and instability effects of super-Alfvénic fast ions that more closely mimics the products of fusion reactions. Recent results from MAST Upgrade are presented, emphasising results that develop the physics basis for spherical tokamaks (STs) and future high beta devices.

2. INTEGRATED PLASMA SCENARIOS

The development of robust, high performance plasma scenarios has underpinned the wider research programme. The integrated scenarios programme has two main goals: to develop reproducible scenarios that maximise confinement of thermal and fast particles and MHD stability, and to develop strongly shaped plasmas with high central safety factor (q_0) to explore stability and confinement with a more reactor-relevant q profile (e.g. compared with STEP [3] and other ST-based concepts [4] and shape of the plasma boundary. In both scenarios, significant effort was dedicated to optimising the early ramp-up phase to tailor the equilibrium q profile.

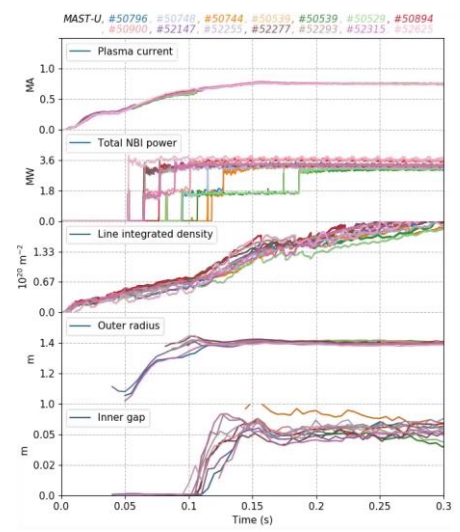


Figure 2: Sensitivity of the ramp-up phase of the high confinement scenario to variation in neutral beam timing, showing that the plasma current evolution (top) and inner and outer radii (bottom) are mostly unaffected by changes in the timing of neutral beam injection (second from top).

In the high confinement scenario, the I_p ramp-up phase was developed with the CREATE-ILC (Iterative Learning Control) tool [5] with the currents in the poloidal field coils and central solenoid placed under feedforward control, transitioning to feedback in the plasma current flat-top phase. The target flat-top plasma current and toroidal field on axis were 0.75 MA and 0.65 T respectively to achieve conditions optimal for studies of plasma exhaust [6] and favourable MHD stability. The ramp-up phase is shown to be very robust to changes in vacuum conditions and the timing of neutral beam injection (see Figure 2). The conditions required for reliable plasma breakdown were guided by the DYON code [7] that has been successfully tested against experiments performed on MAST-U. Internal reconnection events, disruptive events often triggered when the equilibrium q profile exhibits strong reverse shear, have been avoided. Equilibrium shape controllers in the flat-top phase were developed using the TokSys framework [8, 9] to enable fine control of the shape of the plasma core and divertor configuration independently. Careful tailoring of the shape of the last closed flux surface and fuelling of the plasma core are required in Hmode to achieve steady type-I ELMs throughout the flat-top phase. High triangularity and/or squareness can result in a transition to a type-II ELMing regime and low fuelling can result in high pedestal temperatures ($T_{e,ped} > 350 \text{ eV}$) that stimulates a transition to an ELM-free regime (see Figure 3). This transition

is consistent with $n=\infty$ ballooning stability calculations showing that the edge of the plasma is unstable to these modes, which are commonly used as a proxy for kinetic ballooning modes (e.g. [10]), that in turn increases radial transport across the pedestal to avoid triggering ELMs. The thermal and fast ion confinement is limited by m/n = 2/1 tearing modes that are ubiquitous in neutral beam heated H-modes on MAST-U and are described in more detail in section 5.

A high q_0 scenario was developed in parallel with its high confinement counterpart, sharing developments that would benefit the other, as both scenarios have identical flat-top plasma current and toroidal field on axis. The plasma breakdown phase is performed at lower solenoid premagnetisation current to enable the formation of a conventional divertor configuration early in the pulse, from ~40ms after breakdown to reduce the influx of impurities from the inner wall during a limiter phase. The plasma is strongly shaped, with elongation κ ~2.7 during the ramp-up phase, reducing to 2.4-2.5 in the plasma current flat-top. The FreeGSNKE free-boundary equilibrium modelling code [11] was used to guide the development of the plasma current ramp-up phase and calculate equilibrium shape controllers. Strong shaping, coupled with early neutral beam injection, facilitates the formation of a hollow current profile and high q_0 . For example, $q_0 \sim 2.0$ at 0.2s in a typical high confinement scenario compared with 0.4s in the high q_0 scenario. However, the hollow current profile results in a strongly reverse shear q profile that can result in strong internal reconnection events when on-axis and off-axis neutral beam injection is

applied that result in significantly reduced q_0 and can result in termination of the pulse. These reconnection events can be avoided by increasing gas fuelling of the plasma core, which in turn reduces the temperature profile.

The development of alternative divertor configurations was facilitated by use of a new Tokamak Exhaust Designer tool [12]. It represents the flux from the poloidal field coils used to shape the plasma in terms of spherical harmonics, which significantly accelerates the calculations of the coil currents required to produce a given divertor configuration and can accommodate constraints provided by the user, including limits on the allowable coil currents,

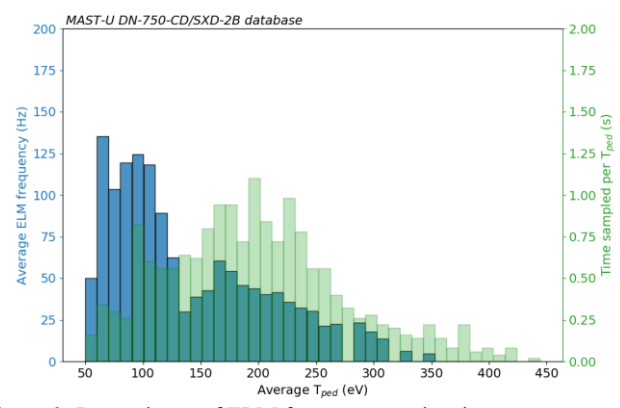


Figure 3: Dependence of ELM frequency on the electron temperature at the top of the pedestal.

position of the separatrix and isoflux surfaces, poloidal flux expansion and radial and vertical magnetic field components, including the position of null points.

3. THERMAL CONFINEMENT

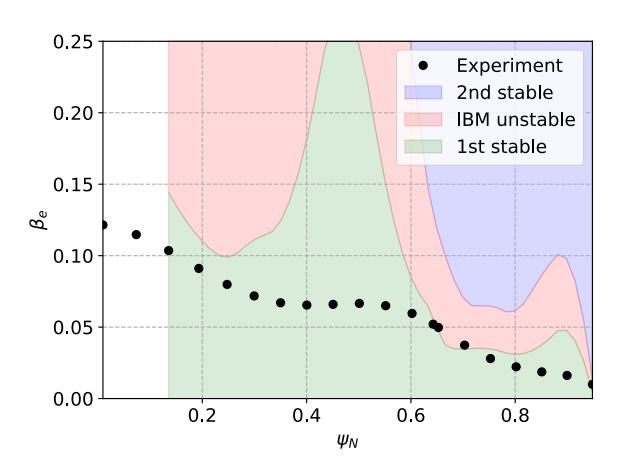


Figure 4: A profile of electron beta, βe , from shot 48657 at 0.6s. The parts of the profile that are stable to ideal ballooning modes (IBM, white), unstable (red) and in the 1st and 2^{nd} stable regions (green and blue respectively) are highlighted.

A significant advantage of low aspect ratio devices is their ability to access high β, offering a potentially economically attractive route to fusion energy production [3]. Predicting energy confinement in high β conditions with gyrokinetic models is challenging, as the electrostatic ion and electron temperature gradient driven modes that can govern confinement at low β can be replaced by electromagnetic instabilities such as microtearing and kinetic ballooning modes (KBM) [13, 14]. Studies on MAST Upgrade have concentrated on accessing high β conditions and characterising turbulent transport to facilitate comparison with predictive simulations. Simulations of turbulent transport in the STEP device [15] predict strong turbulent heat fluxes over a range of β_e $(n_e T_e/(B^2/2\mu_0))$ before reducing to more moderate values at higher β_e . The transition to the

regime with moderate heat fluxes at higher β_e occurs due to the stabilisation of KBM-like modes, which is connected to the ideal ballooning mode (IBM). Simulations of the transition to the moderate heat flux regime are broadly consistent with the stability of the IBM. In a high β experiment performed on MAST Upgrade, shown in Figure 4, it is demonstrated that part of the β e profile lies in a region unstable to ideal ballooning modes where high heat fluxes would be expected in STEP-like conditions. It is posited that MAST Upgrade can access these conditions due to the strong toroidal flows, and flow shear, of current experiments due to strong torque injection from the neutral beams.

4. FAST PARTICLE CONFINEMENT

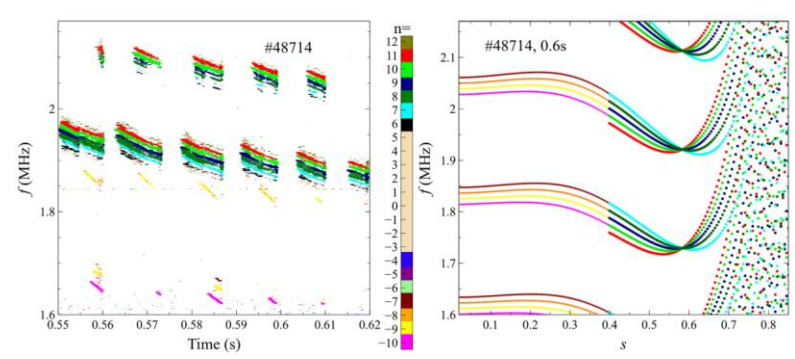


Figure 5: Left: measured frequencies and toroidal mode numbers of modes in the MHz range in pulse number 48714. Right: global Alfvén continua calculated for this pulse at t = 0.6s.

The confinement of energetic particles due to external heating in devices and fusion reactions in future is critical for efficient plasma heating and current drive and to avoid excessive wall loads due to lost fast ions. Modes with frequencies typically ranging from 1-2 MHz (up to around half the on-axis ion cyclotron frequency) are excited in most MAST-U pulses with either SS only or SS + SW NBI and have previously been shown to cause fast ion losses [16]. Analysis of these pulses has

shown that the modes have frequencies lying close to extrema in the global Alfvén eigenmode (GAE) continuum (Figure 5), and eigenmodes at these frequencies have been found using the MISHKA linear ideal MHD code [17]. It is concluded from this analysis that the observed modes are indeed GAEs rather than compressional Alfvén eigenmodes (CAEs).

The appearance of these modes in the ion cyclotron range has motivated work to extend the linear theory of wave-particle interactions to modes of arbitrary frequency [18]. This study indicates that the resonance maps, and hence the expected fast ion losses, associated with GAEs and CAEs in general differ, suggesting that fast ion loss measurements could provide an additional means of distinguishing the two types of mode.

Charge-exchange (CX) with slow edge neutrals is a significant cause of fast ion losses in MAST-U, particularly those originating from the SW beam, and an accurate description of this process is needed for fully quantitative

modelling of plasma performance. To this end, dedicated experiments have been performed using both high-(HFS) and low-field side (LFS) gas fuelling to study CX losses of fast ions [19]. In these pulses a resistive bolometer normally used to record radiation losses was repurposed as a fast neutral diagnostic. The orbit-following ASCOT code, which can model neutralisation and reionisation of the fast ions, was used to simulate the fast neutral power load on the bolometer. In the case of HFS fuelling, a comparison between measured and simulated bolometer loads led to the conclusion that around 10% of the SW beam power was lost due to CX. For LFS fuelling, the comparison is complicated by toroidal asymmetries in the neutral density distribution, but it is clear that the CX losses are much higher in this case, up to about 50% of the SW beam power.

The first measurements of fusion protons have been obtained using a diamond detector that is more resilient to the environment of a fusion device, less sensitive to temperature variations than conventional silicon detectors and offer improved reliability [20]. Considering these findings, an upgraded proton detector has been developed that only contains diamond-based detectors. Measurements of fast ion losses with a Fast Ion Loss Detector have been validated against ASCOT simulations, to enable studies of the interaction of MHD instabilities on fast ion confinement, including type-III ELMs that result in a 25-30% enhancement of fast ion losses from passing orbits [21].

5. MHD STABILITY AND DISRUPTIONS

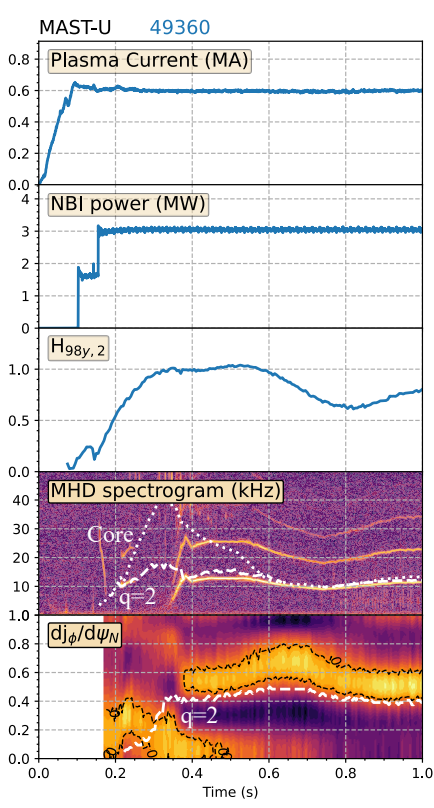


Figure 6: Summary of a typical NBI heated H-mode scenario. An MHD spectrogram (4th sub-figure) shows the toroidal rotation of the plasma core and q=2 flux surface, showing a rapid deceleration of the core rotation after 400ms, when the 2/1 mode appears. The appearance of this mode coincides with the q=2 flux surface being in close proximity to a region where $dJ_{\phi}/d\psi_N=0$.

Studies of MHD stability on MAST Upgrade have concentrated on understanding and avoiding performance-limiting modes towards improving confinement of thermal and energetic species. As mentioned in section 2, m/n = 2/1 modes are commonly observed in neutral beam heated H-mode plasmas and can result in significant degradation of confinement of thermal and fast ions. A summary of a typical pulse exhibiting 2/1 mode activity is shown in Figure 6. The appearance of the mode typically coincides with a strong deceleration of the toroidal rotation at the magnetic axis, matching the rotation velocity at the q=2 flux surface. Once the rotation profiles have stabilised, the stored energy and the stored energy normalised to the ITER IPB98y,2 scaling (H_{98y,2}) [22] can decrease by up to 40% and the neutron rate (not shown) by up to 50%. The onset conditions for 2/1 instabilities on MAST Upgrade are similar to those observed in the DIII-D ITER baseline scenario [23], where the q=2 flux surface is in close proximity to a local minimum in the toroidal current density profile (e.g. where $dJ_{\phi}/d\psi_N = 0$). Experiments have been performed to modify the toroidal current density profile to postpone or avoid the onset of 2/1 modes, including applying vertical shifts and oscillations to modify the profile of the neutral beam driven current and avoiding or delaying the L-H transition with gas fuelling from the low-field side [24] however they have not robustly avoided the onset of these modes. However, these techniques can temporarily disrupt the 2/1 mode, resulting in a transient ~15% increase in β_N before the 2/1 mode is reestablished. As mentioned in section 2, the onset of 2/1 modes can be postponed via developing plasma scenarios optimised to produce an elevated q profile, in particular maximising elongation in the plasma current ramp-up and flat-top phases.

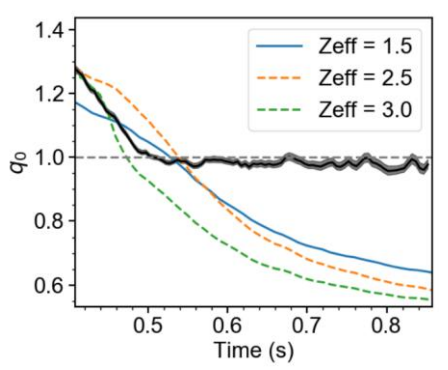


Figure 7: Comparison of the central safety factor, q_0 , inferred from MSE constrained equilibrium reconstruction with estimates from TRANSP, using the NCLASS model of neoclassical current diffusion and different assumptions for the effective charge (Zeff, blue, orange, green)

Understanding and predicting the evolution of the equilibrium q profiles is an important goal of scenario modelling, due to its strong role in governing stability and confinement. Experiments performed with only on- or off-axis neutral beam heating can result in a sawtoothing phase. However, combined on- and off-axis neutral beam injection can facilitate access to a "flux pumping" regime where $q_0 \sim 1$ in the absence of sawteeth [25], in contradiction to neoclassical current diffusion models that predict q₀ drops monotonically below 1 as the current density profile becomes more peaked (a typical MAST Upgrade pulse exhibiting flux pumping is shown in Figure 7). Conditions to access the flux pumping regime in MAST Upgrade include high β_p , high q_{95} and weakly positive magnetic shear close to the magnetic axis. Flux pumping is observed in the presence of m/n = 2/1 modes that are ubiquitous in MAST Upgrade plasmas with strong auxiliary heating.

Operation at high elongation has been demonstrated to be a viable route to improved stability and performance in spherical tokamaks (e.g. [26]). However, ensuring robust vertical stability can be challenging, as the highest sustainable elongation is dependent on ensuring the radial current density profiles in the core are sufficiently broad (or, equivalently, the internal inductance is sufficiently low). This has motivated the development of advanced techniques to predict the radial current density profile, and in turn the vertical stability of strongly shaped plasmas within the DECAF framework [27] that can be applied to real-time control systems. Moreover, DECAF has been applied to the MAST Upgrade dataset to identify the chain of events that can result in a disruptive termination of the plasma [28].

6. PEDESTAL PHYSICS

The edge transport barrier that forms at the periphery of the confined plasma in the high confinement (H-mode) regime offers an attractive route to improved global energy confinement, however the steep pressure gradients can give rise to periodic Edge Localised Mode instabilities that transiently reduce confinement at the edge and elevate divertor power loads [29]. Studies on MAST Upgrade have concentrated on developing fundamental understanding the processes that govern the height and width of the pedestal and avoiding ELMs whilst retaining the benefit of improved confinement in H-mode.

The tightly baffled divertor chambers and flexibility to vary the magnetic configuration within these divertors allows for detailed studies to understand the impact of fuel atoms and molecules interacting with the pedestal arising from the divertor, via either gas fuelling from the divertor or varying the position of the divertor strike point. Initial results from these studies are shown in Figure 8, showing that increasing gas fuelling from the

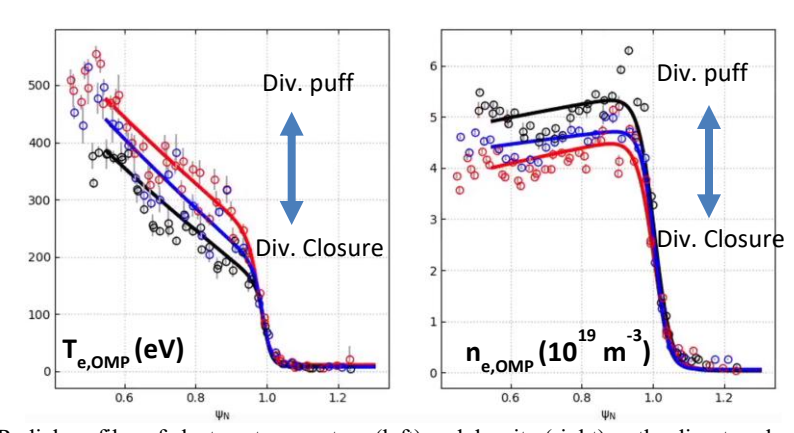


Figure 8: Radial profiles of electron temperature (left) and density (right) as the divertor closure and gas fuelling rate from the divertors are varied, showing that reduced closure, or increased divertor fuelling, reduce the temperature and increase the density at the top of the pedestal.

divertors or decreasing the divertor closure reduce the electron temperature at the pedestal top and elevate the pedestal density profile.

Recent experiments have successfully demonstrated access to small ELM (i.e. type-II ELMs or the Quasi-Continuous Exhaust regime [30]) or stationary ELM-free pedestal regimes as a means of retaining the improved confinement of the H-mode pedestal whilst reducing (or eliminating) transient heat loads from ELMs. It has been demonstrated that strong shaping of the last closed flux surface, specifically a combination of either high squareness or high triangularity, can enable access to a small ELM regime, in qualitative agreement with theoretical predictions [31]. In these experiments, stability modelling performed with the ELITE code [32] indicate that the pedestal is limited by peeling-ballooning modes, predominantly by high-n ballooning modes. As the squareness of the last closed flux surface is increased, a transition from type-I to small ELMs occurs, and the stable region of the peeling-ballooning stability space decreases. Elevated D_{α} emission is observed in the main chamber and Doppler backscattering measurements indicate there is evidence of increased radial particle transport in the pedestal. Access to a small ELM regime has also been demonstrated via strong gas fuelling from the main chamber, which induces a transition from a type-I ELMing regime. Equilibria with self-consistent bootstrap current are found to be unstable to $n=\infty$ ballooning modes near the separatrix in the small ELM regime and are stable to these modes in the type-I ELMing regime, consistent with previous studies [33].

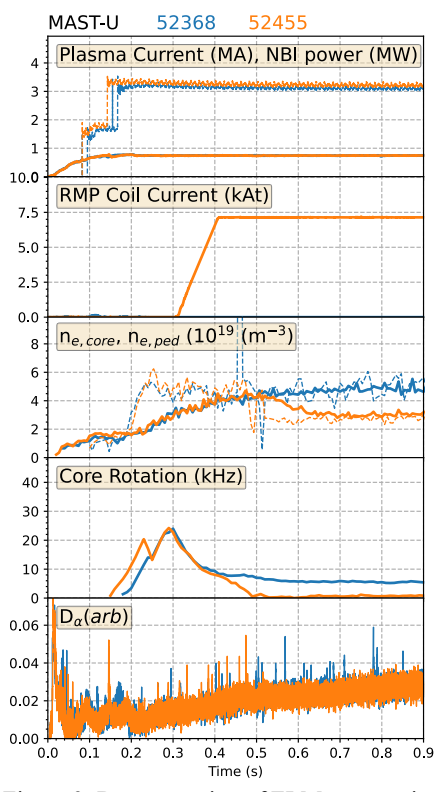


Figure 9: Demonstration of ELM suppression with n=3 RMPs, comparing otherwise similar shots without (blue) and with (orange) RMPs applied. Top – plasma current and neutral beam heating power, 2^{nd} from top – current in the RMP coils, 3^{rd} from top – electron density in the plasma core (solid) and pedestal top (dashed), 4^{th} from top – toroidal rotation at the magnetic axis, bottom – main chamber D_{α} emission.

The application of Resonant Magnetic Perturbations (RMPs) has successfully mitigated type-I ELMs using RMPs with toroidal mode number n=1 with static [34], and more recently, toroidally rotating RMP fields. There has been no evidence of RMPs having a significant effect on ELMs by applying n=2 perturbations, which is thought to be due to the interaction of the RMP with the n=2 component of the intrinsic error field produced by small imperfections in the position, orientation or shape of the poloidal field coils used to shape the plasma. However, the application of n=3 RMPs has resulted in the successful suppression of ELMs for the first time in a spherical tokamak. These experiments were performed in a lower single null topology (most spherical tokamaks operate close to a connected double null topology to minimise the heat flux to the relatively small inner divertors) and are summarised in Figure 9. Comparison of otherwise similar pulses in the presence and absence of n=3 RMPs show that their application results in a reduction in plasma density, from the centre of the plasma to the pedestal top and deceleration of the toroidal rotation, braking the rotation completely and the elimination of ELMs. Thomson scattering measurements of the electron temperature profile indicate the presence of a pedestal when RMPs are applied, confirming that the plasma remains in H-mode.

Initial exploration of negative triangularity scenarios have been performed on MAST Upgrade for the first time in a low aspect ratio device [35], to enable detailed studies of the role of aspect ratio on confinement through comparison with negative triangularity experiments performed on higher aspect ratio devices such as TCV [36] and DIII-D [37]. A transition from type-III ELMing to an ELM-free regime was observed when the radial position of the primary X-points was swept outwards radially, finding that the transition occurs when the average

triangularity (δ_{avg}) is below a critical value, $\delta_{avg} < -0.06$. As triangularity decreases, the electron temperature at the pedestal top also decreases, accompanied by a steady increase in the temperature in the core, thus maintaining $H_{98y,2}$ (\sim 0.7) and β_N (\sim 2) throughout the transition from type-III ELMing to ELM-free regimes. In this experiment, it was found that access to the second stability region for ideal ballooning modes is closed 100ms prior to the

transition to an ELM-free regime, which has not been observed in experiments performed on higher aspect ratio devices.

7. PLASMA EXHAUST

Ensuring adequate power and particle exhaust in large, high power density tokamaks such as ITER and its successors remains a high priority for fusion research. The unique combination of tightly baffled, up-down symmetric divertor chambers that can support conventional and alternative divertor configurations in MAST Upgrade have enabled experiments to study the mechanisms governing divertor detachment and the integration of high-performance core and pedestal regimes with detached divertors. The operational space of MAST Upgrade has recently been expanded with an active cryopump in the lower divertor. Due to the cryopump being situated in the lower tightly baffled divertor chamber, its effect is localised to the lower divertor, as shown in Figure 10.

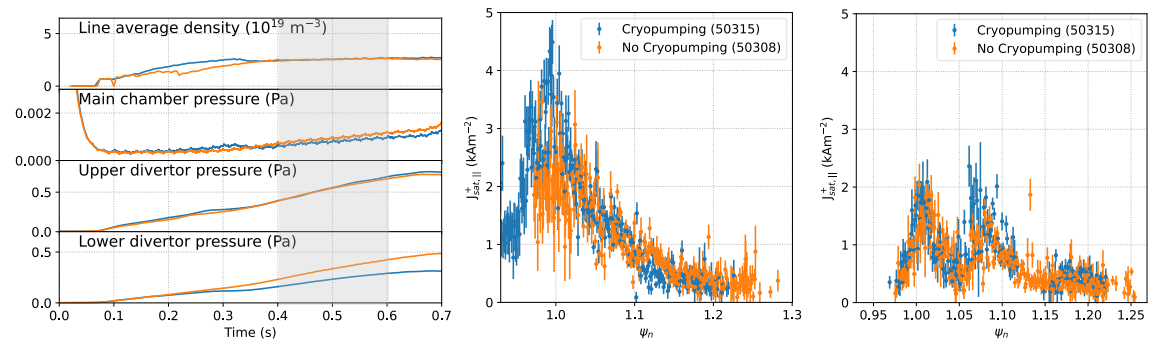


Figure 10: Left - Summary of Ohmic heated experiments with (blue) and without (orange) an active lower divertor cryopump and a Super-X divertor configuration. Between 0.4-0.6s, the line average density and neutral pressures in the upper divertor and main chamber are well matched, but the neutral pressure in the lower divertor is reduced by up to 30%. Middle – outer divertor ion saturation current density profiles from the lower divertor chamber between 0.4-0.6s, showing that the ion flux increases in the presence of cryopumping, indicative of the divertor being less detached. Right – outer divertor ion saturation current density profiles from the upper divertor, taken over the same period as for the lower divertor, which are unaffected by the lower divertor cryopump.

Studies of the impact of the cryopump and fuelling location on the outer mid-plane separatrix density have been performed in experiments and compared with SOLPS-ITER simulations [38]. In experiments with conventional and Super-X divertor configurations, with fuelling predominantly from the divertor chambers, a dependence of the separatrix density ($n_{e,sep}$) on divertor neutral pressure (P_n) is found $n_{e,sep} = 0.71 \times P_n^{0.3}$, in good agreement with simulations that yield a similar trend $n_{e,sep} = 0.69 \times P_n^{0.34}$, in qualitative agreement with trends observed on other devices, [39, 40]. Conversely, experiments performed with fuelling from the high-field side yield a higher exponent, $n_{e,sep} = 2.83 \times P_n^{0.62}$, which is notably different than the trend recovered from simulations $n_{e,sep} = 1.22 \times P_n^{0.83}$.

The Super-X divertor configuration [41] greatly facilitates access to the detached divertor regime [6, 42], such that the outer divertors are typically detached over the operating space of MAST Upgrade with minimal impact on the edge pedestal or plasma core. The plasma conditions in the divertor chambers in the Super-X configuration are typically low temperature ($T_e < 1 \text{ eV}$) and low density ($n_e < 1 \times 10^{19} \text{ m}^{-3}$), where plasma-molecule interactions can result in significant dissipation of particles, momentum and energy [42]. Measurements of D_2 Fulcher band emission in MAST Upgrade and TCV have been used to infer the rotational temperature of D_2 molecules [43], showing that as the separatrix density increases and the outer divertors are more deeply detached, the rotational temperature of D_2 molecules increases, suggesting that the plasma is transferring energy to D_2 molecules in the divertors. However, the complexity of plasma-molecule interactions, with sufficient resolution to capture the rovibrational states of D_2 , is challenging to incorporate in multi-fluid simulations such as SOLPS-ITER. Simulations have been performed with SOLPS-ITER of detachment onset and evolution in MAST Upgrade-like conditions in simplified geometry [44] with models of plasma-molecule interactions of increasing fidelity. Higher fidelity models of plasma-molecule interactions predict a ~20% reduction in the upstream separatrix density required to detach the outer divertor leg, due to higher rates of molecular charge-exchange $(p + H_2 \rightarrow H + H_2^+)$, thus

elevating the density of molecular ions, leading to higher rates of molecular activated recombination and molecular activated dissociation.

Studies of core-edge-divertor integration were initially performed with the outer divertors in the Super-X configuration [6] and have recently been extended to study the X-point target [45]. These experiments show qualitatively similar behaviour as those performed in the Super-X configuration, indicating detached conditions at the outer divertor targets while having minimal impact on the edge pedestal or plasma core ($T_{e,core} \sim 1 \text{ keV}$, $T_{e,ped} \sim 0.2 \text{ keV}$, $H_{98y,2} \sim 0.7$ -0.8, $\beta_N \sim 2.5$). However, divertor Thomson scattering measurements indicate the electron temperature in the lower divertor is reduced in the X-point target configuration compared with an otherwise similar experiment with a Super-X configuration. Measurements of 2D electron density profiles via coherence imaging spectroscopy [46] in otherwise similar experiments with Super-X and X-point target configurations (see Figure 11), show that, while the peak electron density is similar, the radial width of the density profiles is higher in the X-point target configuration due to the higher poloidal flux expansion and the electron temperature is generally lower compared with the Super-X configuration, which is thought to be due to stronger plasma-neutral interactions.

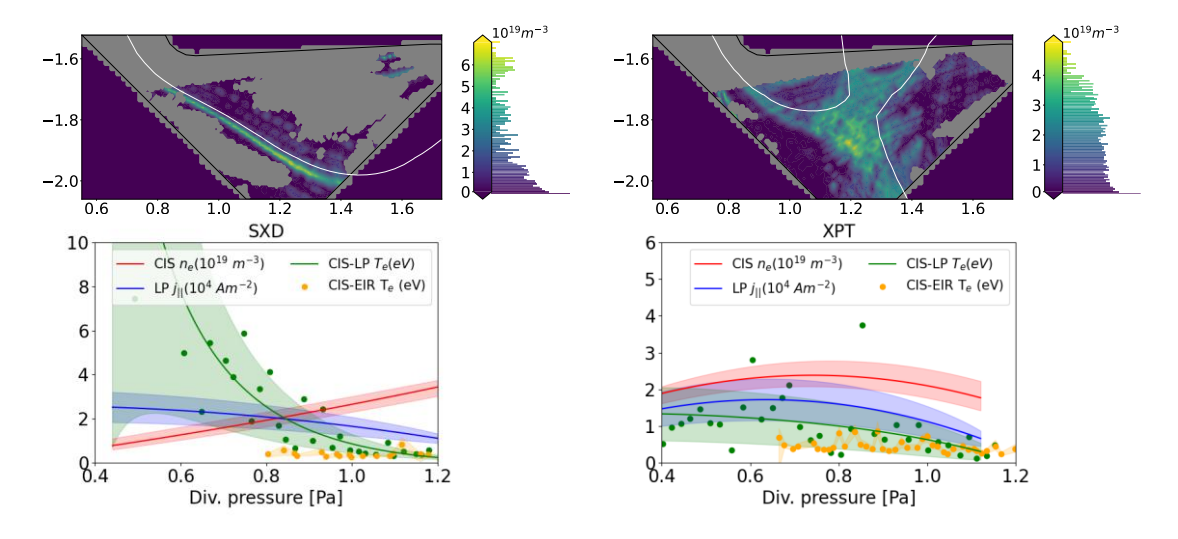


Figure 11: Left top - 2D n_e profile in a Super-X divertor configuration with the equilibrium separatrix overlaid, left bottom - inferred electron density (red), temperature (green, yellow) and ion saturation current density (blue) profiles. Right top, bottom – profiles measured in the X-point target configuration, with the same layout as the plots on the left.

A substantial predicted benefit of alternative divertor configurations is improved controllability of divertor detachment [47], leveraging gradients in B (referred to here as "total flux expansion", which in turn lead to gradients in the parallel heat flux) to passively stabilise the movement of the detachment front. These predictions were tested in system identification studies [48] using a sinusoidally varying fuelling rate from the divertor chambers to measure its impact on the detachment front, via multi-wavelength imaging of D₂ Fulcher band emission. Divertor configurations with the greatest total flux expansion exhibited the weakest response, while divertor configurations with lower total flux expansion showed stronger response. The detachment state of each divertor can be varied independently when the plasma is close to a connected double null topology, such that the upper and lower outer divertors are connected via magnetic field lines. This behaviour is not commonly observed in present day experiments, but is expected to manifest in future devices such as STEP, which is currently designed with up-down symmetric, tightly baffled divertors in common with MAST Upgrade. Building on these system identification studies, real-time control of the detachment front position in the lower divertor chamber, inferred via real-time analysis of D₂ Fulcher band emission detected with the Multi-Wavelength Imaging system, has been successfully demonstrated, using gas fuelling as the actuator. The real-time detachment control capability was applied to characterise the dynamics of divertor detachment and subsequent re-attachment, by increasing and decreasing fuelling rates respectively, showing that the timescales for re-attachment are shorter when the lower divertor cryopump is active. Coverage of the Multi-Wavelength Imaging systems and detachment control capabilities have been extended to the upper divertor chamber, allowing for simultaneous control of the detachment states of both divertors independently of each other and the density of the plasma core.

8. HARDWARE ENHANCEMENTS AND FUTURE PROGRAMME

A programme of enhancements is underway to expand the operational space of MAST Upgrade towards more reactor-relevant conditions, including higher beta and lower collisionality in the plasma core and edge pedestal and to increase the heat flux entering the divertors to facilitate more stringent tests of the power handling capabilities of conventional and alternative divertor configurations. In 2027, two additional neutral beam injectors will be installed, both with a maximum injected power of 2.5 MW, one with a similar injection geometry as the existing off-axis beam, and the other will be intermediate between the existing on-axis and off-axis beams. This will double the neutral beam heating power available and provide significant flexibility to vary the fast ion pressure profiles to avoid energetic particle driven instabilities. In parallel, a 1.8 MW electron Bernstein wave (EBW) heating and current drive system is being developed [49], with injection frequencies of 28 GHz and 34.8 GHz to enable studies EBW mode conversion and current drive efficiency in on-axis and off-axis injection geometries, in support of the STEP physics mission. A high frequency pellet injector will be commissioned to enable studies of the impact of pellet fuelling on confinement and the development of power exhaust solutions that can accommodate modulations in plasma density due to pellet injection.

The future MAST Upgrade research programme will utilise these new capabilities to study thermal energy confinement at higher electron toroidal beta and the effects of toroidal rotation by varying the power injected from the neutral beam and EBW systems, and hence the net torque coupled to the plasma. Operation at higher heating power is expected to enable studies of MHD stability at values of β exceeding the no-wall stability limit [50], motivating the development of techniques to stabilise or control resistive wall modes. Studies of plasma exhaust and scenario integration will be extended to higher heat flux, enabling more detailed exploration of the onset of divertor detachment in alternative divertor configurations such as the Super-X and X-point target and more extensive use of impurity seeding to vary the degree of detachment of each divertor. As more diagnostics provide more real-time data output, the control capabilities of MAST Upgrade will expand to facilitate comparison of techniques to control plasma properties and the equilibrium in the main chamber and in the divertors. Initial studies of EBW heating and current drive will concentrate on power deposition and current drive to develop deeper understanding of EBW mode conversion and the role of Ohkawa and Fisch-Boozer current drive mechanisms and their dependences on plasma operating scenarios to test predictive models.

ACKNOWLEDGEMENTS

This work has been carried out within the framework of the EUROfusion Consortium, funded by the European Union via the Euratom Research and Training Programme (Grant Agreement No 101052200 — EUROfusion) and from the EPSRC [grant numbers EP/W006839/1]. To obtain further information on the data and models underlying this paper please contact PublicationsManager@ukaea.uk. Views and opinions expressed are however those of the author(s) only and do not necessarily reflect those of the European Union or the European Commission. Neither the European Union nor the European Commission can be held responsible for them.

REFERENCES

- [1] J W Berkery et al. Plasma Phys. Control. Fusion 67 053001 (2025)
- [2] H. Zohm et al. Nucl. Fusion 53 073019 (2013)
- [3] H. Meyer et al. Phil. Trans. R. Soc. A 382 20230406 (2024)
- [4] J. E. Menard et al. Nucl. Fusion 56 106023 (2016)
- [5] L. E. di Grazia, et al. Iterative learning optimization and control of MAST-U breakdown and early ramp-up scenarios. Optim Eng (2025)
- [6] J R Harrison et al Plasma Phys. Control. Fusion 66 065019 (2024)
- [7]. H. T. Kim this conference
- [8] H. Anand et al Nucl. Fusion 64 086051 (2024)
- [9] A Lvovskiy et al Plasma Phys. Control. Fusion 67 075003 (2025)
- [10] J.F. Parisi et al Nucl. Fusion 64 054002 (2024)
- [11] N. C. Amorisco Phys. Plasmas 31, 042517 (2024)

IAEA-CN-316/2808

- [12] O. P. Bardsley et al., Plasma Phys. Control. Fusion 66 055006 (2024)
- [13] S M Kaye et al Plasma Phys. Control. Fusion 63 123001 (2021)
- [14] D. Kennedy et al Nucl. Fusion 63 126061 (2023)
- [15] D. Kennedy et al., this conference
- [16] J. F. Rivero-Rodríguez et al. Nucl. Fusion 64 086025 (2024)
- [17] M. B. Dreval et al. Nucl. Fusion 65 016043 (2025)
- [18] M. Fitzgerald, B. N. Breizman Fundamental Plasma Physics 13 100084 (2025)
- [19] P. Ollus et al. Plasma Phys. Control. Fusion 67 055039 (2025)
- [20] A. Aboutaleb et al., Rev. Sci. Instrum. 95, 083522 (2024)]
- [21] L. Velarde et al., Plasma Phys. Control. Fusion 67 015024 (2025)
- [22] O. Kardaun, Plasma Phys. Control. Fusion 41 429 (1999)
- [23] F. Turco et al Nucl. Fusion 58 106043 (2018)
- [24] M. Valovic, et. al., Plasma Phys. Contr. Fusion 44 (2002) A175
- [25] S. Blackmore et al. this conference
- [26] S.P. Gerhardt et al., Nucl. Fusion 51 073031 (2011)
- [27] M. Tobin et al., Plasma Phys. Control. Fusion 66 105020 (2024)
- [28] V. Zamkovska et al., Nucl. Fusion 64 066030 (2024)
- [29] T. Eich et al., Nucl. Mater. Energy 12 84-90 (2017)
- [30] M.E. Fenstermacher et al., Nucl. Fusion 65 053001 (2025)
- [31] J. Parisi et al., arXiv, https://arxiv.org/abs/2505.02727 (2025)
- [32] H. R. Wilson and S. C. Cowley, Physical Review Letters 92 (2004)
- [33] M. Dunne et al., Nucl. Fusion 64 124003 (2024)
- [34] D. A. Ryan et al Plasma Phys. Control. Fusion 66 105003 (2024)
- [35] A.O. Nelson et al., Nucl. Fusion 64 124004 (2024)
- [36] S. Coda et al., Plasma Phys. Control. Fusion 64 014004 (2022)
- [37] K. E. Thome et al., Plasma Phys. Control. Fusion 66 105018 (2024)
- [38] Q. Xia, this conference
- [39] A Kallenbach et al., Plasma Phys. Control. Fusion 60 045006 (2018)
- [40] L. Frassinetti et al., Nucl. Fusion 61 016001 (2021)
- [41] P. M. Valanju et al. Phys. Plasmas 16 056110 (2009)
- [42] K. Verhaegh et al. Nucl. Fusion 63 016014 (2023)
- [43] N Osborne et al. Plasma Phys. Control. Fusion 66 025008 (2024)
- [44] J. Bryant et al., Nucl. Fusion 65 036025 (2025)
- [45] B. LaBombard et al. Nucl. Fusion 55 053020 (2015)
- [46] N Lonigro et al. Plasma Phys. Control. Fusion 67 035003 (2025)
- [47] B. Lipschultz et al. Nucl. Fusion 56 056007 (2016)
- [48] B. Kool et al. Demonstration of Super-X divertor exhaust control for transient heat load management in compact fusion reactors. Nat Energy (2025)
- [49] P. Jacquet this conference
- [50] J. W. Berkery et al. Plasma Phys. Control. Fusion 62 085007 (2020)